Part I

Advances in the Structure and Chemistry of Sepiolite and Palygorskite

Chapter 1

The Structures and Microtextures of the Palygorskite–Sepiolite Group Minerals

Stephen Guggenheim* **and Mark P.S. Krekeler†**

**Department of Earth and Environmental Sciences, University of Illinois at Chicago, Chicago, Illinois, USA*

†Department of Geology, Miami University Hamilton, Hamilton, Ohio, USA

1. INTRODUCTION

Although palygorskite–sepiolite minerals are closely related to chain silicates or represent transitional phases between chain silicates and layer silicates (e.g. the biopyriboles, Zoltai, 1981), their affinities to the (layer) phyllosilicates are a valuable asset in comparative crystal chemistry. Bailey (1980), and to a much lesser extent Guggenheim and Eggleton (1988), made comparisons of palygorskite and sepiolite to ideal phyllosilicates or modulated phyllosilicates, respectively. Since this earlier work, additional members of the palygorskite–sepiolite group or related minerals have been discovered and their atomic structures have been refined by single-crystal techniques. Authors of these single-crystal studies recognized and commented on the relationships of these structures to phyllosilicates in general and palygorskite and sepiolite in particular. However, they did not analyze in detail the relationship of these minerals as a group to relate crystal chemistry, structure, and geologic origin. This chapter, although limited by length, develops an initial cogent comparison of the palygorskite–sepiolite group minerals to modulated phyllosilicates by considering these relationships. In addition, a summary of the literature on the microstructure of palygorskite and sepiolite is included. Portions of this chapter were presented in abstract form by Guggenheim (2010).

Developments in Clay Science, Vol. 3. DOI: 10.1016/B978-0-444-53607-5.00001-3

2. PART 1. STRUCTURE-RELATED TOPICS

2.1. Structural Characteristics of the Palygorskite–Sepiolite Mineral Group

Like all ideal phyllosilicate minerals containing 2:1 layers where there is an octahedral sheet between two opposing tetrahedral sheets, the palygorskite–sepiolite minerals have continuous planes of tetrahedral basal oxygen atoms approximately 6.6 Å apart (e.g. Bailey, 1980). However, unlike the ideal 2:1 phyllosilicates, the apical oxygen atoms point away from the basal oxygen atom plane in opposing directions to form ribbons of joined pyroxene-like chains (e.g. Figure 1, details of specific species given below). The apical

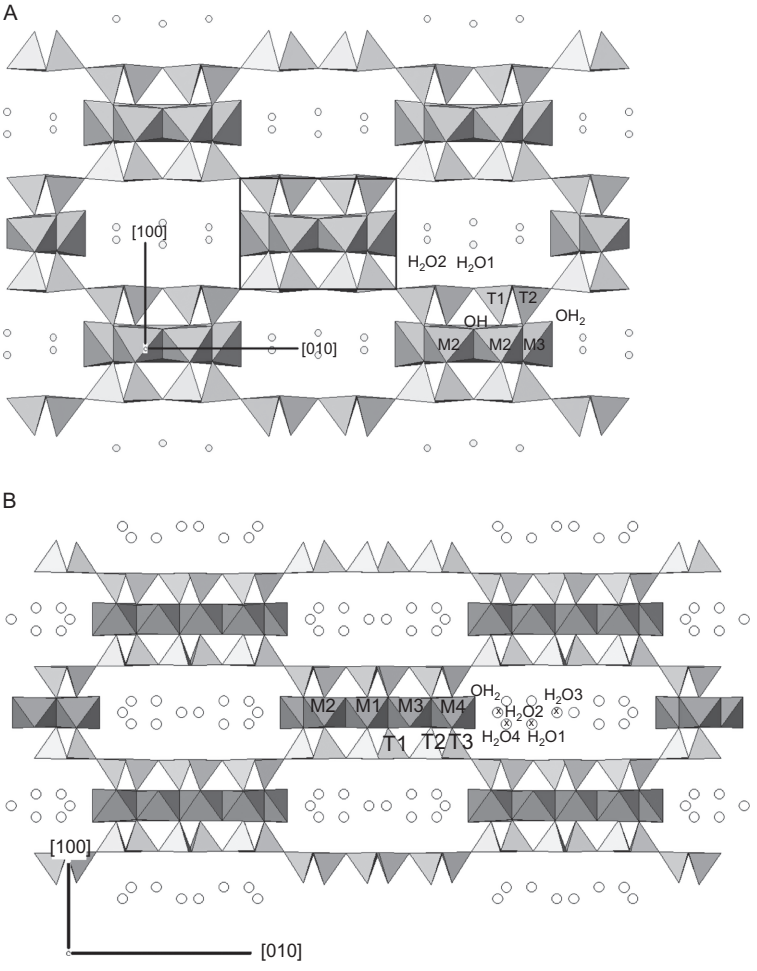

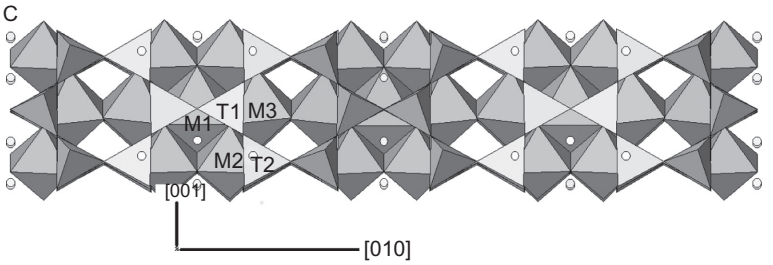

FIGURE 1 Projection of the monoclinic palygorskite (A) and sepiolite (B) structures along the [001] direction. The box in the centre of (A) illustrates a polysome. All figures show polyhedral representations. Octahedral metal cations (commonly Mg, Al) are shown as dark-fill octahedra (grey for online version), and Si-containing tetrahedra are shown as lighter-fill triangles (yellow for online version). Octahedral cation sites (M) and tetrahedral cation sites (T) are labelled. In (A), the M1 site (not shown) is located between and in front of the two labelled M2 sites in this projection; see (C) for additional site identification. Open circles are zeolitic H_2O. In sepiolite (B), M2 is slightly behind M1, which is slightly behind M3 in this projection. Open circles are zeolitic H_2O, with those marked "x" being labelled. (C) Projection of palygorskite along the [100] direction. The tetrahedral sheet, with sixfold rings, is an essential feature in the palygorskite–sepiolite mineral group. Coordinates from Post and Heaney (2008) and Post et al. (2007). Plotting programme ATOMS (Dowty, 2005) was used to create all figures. (For interpretation of the references to colour in this figure legend, the reader is referred to the Web version of this chapter.)

oxygen atoms of the tetrahedra partially form the coordination unit of the octahedral sheet. Therefore, there is a region of the structure where a channel may form adjacent to the basal oxygen planes between two 2:1 layers, for example, in palygorskite and sepiolite. Guggenheim and Eggleton (1988) proposed a 'modulated' phyllosilicates classification scheme, with palygorskite and sepiolite as members because of the inverted tetrahedral arrangement and the formation of the channel where the octahedral sheet becomes discontinuous. This classification scheme was extended and adopted by the Clay Minerals Society (Martin et al., 1991) and included in a summary of recommendations of nomenclature committees relevant to clay mineralogy presented by Guggenheim et al. (2006, Table 3). The essential features of the palygorskite–sepiolite mineral group are apparently (1) the continuous tetrahedral basal oxygen planes, (2) the inverted tetrahedral arrangement that forms ribbons of joined pyroxene-like chains, and (3) the discontinuous octahedral sheet.

The description of the palygorskite–sepiolite mineral *group* has, in the past, involved the minerals palygorskite and sepiolite as model structures because there was no need to consider other possible models. Since 1991, several minerals closely associated to palygorskite and sepiolite have been described and their structures were determined, for example, intersilite (Khomyakov, 1995; Yamnova et al., 1996), kalifersite (Ferraris et al., 1998), raite

(Khomyakov, 1995; Pluth et al., 1997), and tuperssuatsiaite (Cámara et al., 2002; Karup-Møller and Peterson, 1984). Tuperssuatsiaite and raite have all the essential features of the group, and they are clearly members. Because a structure refinement is unavailable, it is unclear if kalifersite (Ferraris et al., 1998) merits membership, but provisional analysis by Ferraris et al. (1998) suggests that it should be tentatively assigned to the group. For intersilite, the configuration of the chains is not "pyroxene-like", and thus this mineral should be considered a "related" mineral. This chapter includes intersilite for comparison where possible, but the different chain geometry makes many comparisons difficult.

2.2. Species and Nomenclature

The palygorskite–sepiolite group (Table 1) consists of palygorskite, sepiolite, falcondoite, kalifersite, loughlinite, raite, tuperssuatsiaite, and yofortierite. Intersilite is given in the table for comparison. Each mineral of Table 1 is trioctahedral, except for palygorskite and its Mn analogue, yofortierite, which are dioctahedral. "Attapulgite" was a name introduced by de Lapparent (1935) for a fibrous clay found near Attapulgus, Georgia, USA, but the name was subsequently discredited by the International Mineralogical Association

TABLE 1 Palygorskite–Sepiolite Group Minerals and Intersilite.

Mineral	Formula	Reference
Falcondoite	$\sim(Ni_{8-y-z}R^{3+}{}_y\square_z)(Si_{12-x}R^{3+}{}_x)$ $O_{30}(OH)_4(OH_2)_4{\cdot}R^{2+}{}_{(x-y+2z)2}(H_2O)_8$	Modified from Springer (1976)
Intersilite	$(Na_{0.80}K_{0.45}\square_{0.75})Na_5Mn(Ti_{0.75}Nb_{0.25})$ $[Si_{10}O_{24}(OH)]{\cdot}(O,OH)(OH)_2{\cdot}4H_2O$	Yamnova et al. (1996)
Kalifersite	$(K,Na)_5Fe^{3+}{}_7(Si_{20}O_{50})(OH)_6{\cdot}12(H_2O)$	Ferraris et al. (1998)
Loughlinite	$\sim Na_4Mg_6(Si_{12}O_{30})(OH)_4(OH_2)_4$	Fahey et al. (1960)
Palygorskite	$\sim(Mg_{5-y-z}R^{3+}{}_y\square_z)(Si_{8-x}R^{3+}{}_x)$ $O_{20}(OH)_2(OH_2)_4{\cdot}R^{2+}{}_{(x-y+2x)/2}(H_2O)_4$	Drits and Aleksandrova (1966)
Raite	$\sim Na_3Mn_3Ti_{0.25}(Si_8O_{20})(OH)_2{\cdot}10(H_2O)$	Pluth et al. (1997)
Sepiolite	$\sim(Mg_{8-y-z}R^{3+}{}_y\square_z)(Si_{12-x}R^{3+}{}_x)$ $O_{30}(OH)_4(OH_2)_4{\cdot}R^{2+}{}_{(x-y+2z)/2}(H_2O)_8$	Bailey (1980)
Tuperssuatsiaite	$\sim Na_{1.87}Fe_{2.14}Mn_{0.48}Ti_{0.14}\ (Si_8O_{20})(OH)_2{\cdot}n$ (H_2O)	Cámara et al. (2002)
Yofortierite	$\sim(Mn_{5-y-z}R^{3+}{}_y\square_z)(Si_{8-x}R^{3+}{}_x)$ $O_{20}(OH)_2(OH_2)_4{\cdot}R^{2+}{}_{(x-y+2x)/2}(H_2O)_4$	Modified from Perrault et al. (1975)

The □ symbol denotes vacancy.

(IMA) because palygorskite, which was reported from the Palygorsk Range, Ural Mountains, Russia, in 1862 (Ssaftschenkow, 1862), has precedence. Robertson (1962) suggested the name "hormite" for the palygorskite–sepiolite group, but this name was not accepted by the IMA. Unfortunately, the terms "attapulgite" and "hormite" are still commonly used in industry journals. The name "palysepioles" was introduced by Ferraris et al. (1998) in reference to a "palysepioles polysomatic series" with the "palysepioles" as members of the palygorskite–sepiolite series, but this name was rejected by the Association Internationale pour l'Etude des Argiles (AIPEA) Nomenclature Committee as unnecessary.

2.3. Structure of the Palygorskite–Sepiolite Mineral Group and Related Minerals

Single-crystal X-ray analyses of palygorskite and sepiolite are not available, but the overall structures have been obtained from powder-data studies. These studies (Artioli et al., 1994; Chiari et al., 2003; Chrisholm, 1992; Christ et al., 1969; Drits and Sokolova, 1971; Giustetto and Chiari, 2004; Post and Heaney, 2008) confirmed the basic structure of Bradley (1940) for palygorskite (for summaries of previous models, see Bailey, 1980 and Jones and Galán, 1988). The known structural modifications are monoclinic ($C2/m$) and orthorhombic ($Pbmn$); these modifications are commonly intergrown. Rietveld refinement procedures were applied to palygorskite by Artioli et al. (1994), Chiari et al. (2003), Giustetto and Chiari (2004), and Post and Heaney (2008). Like the ideal phyllosilicates, the palygorskite–sepiolite group has an overall structure where there are infinitely extending tetrahedral sheets involving sixfold rings of tetrahedra. These tetrahedral sheets have a continuous basal oxygen atom plane but, unlike the ideal phyllosilicates, the palygorskite–sepiolite group has apical oxygen atoms pointing along either the [100] or the [$\bar{1}$00] direction, that is, in opposing directions (Figure 1). The apical oxygen atoms form a strip or ribbon pattern such that the strip extends along the [001] direction; the width of the apical oxygen atom strip consists of a tetrahedral ring (or two pyroxene-like chains) in palygorskite, tuperssuatsiaite, and raite, and 1.5 rings (or three pyroxene-like chains) in sepiolite. Strips with apices pointing in one direction link to metal cations (typically Mg or Al in palygorskite and sepiolite) to form a portion of the octahedral coordination. The remaining part of the coordination unit is completed by apical oxygen atoms of an opposing tetrahedral strip and by two OH groups (or by OH_2 groups in special cases, see below). Thus, two apical oxygen atoms are obtained from one strip, two additional apical oxygen atoms are from the opposing strip, and two OH groups complete most octahedra. Strips that are eight octahedra wide link to tetrahedra via apical oxygen atoms in sepiolite, and strips that are five octahedra in width occur in palygorskite. Thus the octahedra do not form continuous sheets. The

combination of an octahedral strip and adjacent strips of tetrahedra form a "polysome" which, when compared to an ideal phyllosilicate, resembles the 2:1 layer, although more limited in lateral extent (Figure 1). The basal oxygen atom plane to basal oxygen atom plane spacing is about 6.5 Å, which is similar to that found in mica.

Structural information from Rietveld refinements (Table 2) is generally less precise than single-crystal refinements (see Post and Bish, 1989), and the lack of such precision is commonly observed in the reported bond distances, with associated errors about a magnitude larger than those reported from a typical single-crystal refinement; bond lengths are paramount in determining site occupancy and distortions. In part, obtaining a reasonable result in Rietveld refinements often involves fixing (or limiting the variation of) atomic parameters, which may establish the size and shape of polyhedra, and this was done to some extent for all Rietveld refinements (constraints are noted in Table 2). Although the lack of precision of individual bond distances and angles inhibits detailed interpretation of structural data, *average* polyhedral sizes from Rietveld refinements tend to be similar to those obtained from single-crystal data, even for polyhedra that are not constrained. Thus, consideration of structural parameters, which generally involve averaging, is probably more fruitful than direct comparisons of individual distances and angles.

Single-crystal X-ray studies (Table 3) have been performed on raite (Pluth et al., 1997) and tuperssuatsiaite (Cámara et al., 2002). Both minerals have palygorskite-like Si tetrahedral frameworks, and both contain Na, Mn, and Ti, but tuperssuatsiaite is Fe rich. The octahedral backbone in raite (Figure 2) consists of a continuous strip of Mn octahedra (Mn1, Mn2) along the [001] direction with appendages of Na octahedra (Na1) on either side of the strip to form the octahedral part of the polysome. Polysomes are weakly connected laterally by channels containing vacant regions, isolated Na octahedra (Na2), and partially occupied (1/9 occupancy) distorted Ti octahedra linking the Na2 and the Mn2 and Na1 octahedra. Like palygorskite, strong polysome connectivity is obtained by the cross-linking tetrahedral rings with apical oxygen atoms that belong also to the coordination of the M1 and M2 octahedra.

Intersilite (Yamnova et al., 1996) is similar to the members of the palygorskite–sepiolite group in that there are continuous planes of basal oxygen atoms which form polysomes involving an octahedral strip (Mn, Na, and Ti + Nb) and coordinating tetrahedra (not illustrated). In contrast, however, the tetrahedral configuration within the polysome is composed of both six- and eightfold rings normal to the [100] direction, with polysomes connected by fivefold rings. Also, there are regions of partially occupied (with K, Na) seven- and eight-coordinated polyhedra that alternate with polysomes along both the [010] and [100] directions. Although this polysome configuration is similar to that of the palygorskite–sepiolite group minerals, the

TABLE 2 Powder (Rietveld) Refinements and Derived Structural Parameters.

Species	Reference	Space group	Final R_{wp} (m, multiphase)[a]	$\alpha_{polysome}$ (°)	$\alpha_{interpolysome}$ (°)
1. Sepiolite	Post et al. (2007)	*Pncn*	0.021	2.20	2.46
2. Palygorskite	Post and Heaney (2008)	*C*2/*m*	0.022	0.81	0.53
3. Palygorskite	Giustetto and Chiari (2004)	*C*2/*m*	0.043 (m)	12.62	10.82
4. Palygorskite	Chiari et al. (2003)	*C*2/*m*	6.33	11.79	8.28
5. Palygorskite	Artioli and Galli (1994)	*C*2/*m*	0.130 (m)	12.43	8.64
6. Palygorskite	Giustetto and Chiari (2004)	*Pbmn*	0.043 (m)	5.72	8.63
7. Palygorskite	Artioli and Galli (1994)	*Pbmn*	0.130 (m)	6.72	8.11

Species	Average bond distances (Å)		$\psi_{octahedron}$ (°)	Oct. thickness (Å)	τ (°)	Tet. thickness (Å) *Average*[b]	*b*/2 (Å)[c]
1. Sepiolite	M1: 2.077	T1: 1.634	M1: 58.2	M1: 1.192	T1: 111.3	2.216	9.005
	M2: 2.062	T2: 1.635	M2: 58.8	M2: 2.137	T2: 113.3		
	M3: 2.084	T3: 1.620	M3: 58.3	M3: 2.157	T3: 110.7		
	M4: 2.085		M4: 57.8	M4: 2.224			
2. Palygorskite	M1: 2.158[d]	T1 1.622	M1: 61.3[d]	M1: 2.075	T1: 110.4	2.412	8.925
	M2: 1.873	T2 1.624	M2: 57.0	M2: 2.041	T2: 112.9		
	M3: 2.087		M3: 55.6	M3: 2.360			

Continued

TABLE 2 Powder (Rietveld) Refinements and Derived Structural Parameters.—Cont'd

Species	Average bond distances (Å)		$\psi_{octahedron}$ (°)	Oct. thickness (Å)	τ (°)	Tet. thickness (Å) *Average*[b]	*b*/2 (Å)[c]
3. Palygorskite	M1: 2.497	T1: 1.644	M1: 64.7	M1: 2.136	T1: 106.7	1.874	8.940
	M2: 2.128	T2: 1.649	M2: 58.3	M2: 2.239	T2: 106.9		
	M3: 2.151		M3: 57.8	M3: 2.290			
4. Palygorskite	M1: 2.219	T1: 1.648	M1: 63.9	M1: 1.951	T1: 113.9	1.938	8.938
	M2: 2.133	T2: 1.665	M2: 59.8	M2: 2.146	T2: 107.2		
	M3: 2.312		M3: 64.0	M3: 2.027			
5. Palygorskite	M1: 2.235	T1: 1.647	M1: 61.1	M1: 2.162	T1: 119.4	2.006	8.934
	M2: 2.097	T2: 1.661	M2: 57.2	M2: 2.272	T2: 106.7		
	M3: 2.311		M3: 62.1	M3: 2.162			
6. Palygorskite	M1: 2.263	T1: 1.635	M1: 58.7	M1: 2.349	T1:108.5	2.193	8.938
	M2: 2.053	T2: 1.635	M2: 58.9	M2: 2.121	T2: 100.3		
	M3: 2.116		M3: 57.4	M3: 2.281			
7. Palygorskite	M1: 1.724	T1: 1.629	M1: 70.1	M1: 1.174	T1: 98.7	1.130	8.921
	M2: 1.941	T2: 1.631	M2: 67.7	M2: 1.475	T2: 108.8		
	M3: 2.064		M3: 66.6	M3: 1.637			

[a]*Constraints/procedures used during refinement: 1 and 2, T—O bonds, "soft" constraints, but not fully removed at end of refinement; 3 and 6, soft constraints (=constraints removed at end of refinement) on T—O and M—O bonds, refinement matrix uncoupled to lower correlations, hard constraints on thermal (displacement) parameters; 4, soft constraints on T—O, M—O bonds and angles, refinement matrix uncoupled to lower correlations; 5 and 7, constraints, if any, not given.*
[b]*Includes OH, but not the oxygen atom on special position 1/4, 1/4, z, or OH_2.*
[c]*Sepiolite value normalized to 4 tetrahedra per polysome. Value for falcondoite, normalized to 4 tetrahedra per polysome, is 8.967; the value for yofortierite, assuming that the 4.41 diffraction line is indexed as the 040 is 8.82; and the value for loughlinite is 8.90 Å, assuming that the 4.45 diffraction line is the 040.*
[d]*M sites redefined from Post and Heaney (2008), M1 is the vacant site.*

TABLE 3 Single-Crystal Refinements and Derived Structural Parameters of Palygorskite-like Minerals.

Species	Reference	Space group	# obs. reflections	Final R_1	$\alpha_{polysome}$ (°)	$\alpha_{interpolysome}$ (°)
Tuperssuatsiaite	Cámara et al. (2002)	*C*2/*m*	905	0.075	1.99	1.57
Raite	Pluth et al. (1997)	*C*2/*m*	1164	0.07	5.09	3.70

Species	Average bond distances (Å)		$\psi_{octahedron}$ (°)	Oct. thickness (Å)	τ (°)	Tet. thickness (Å) *Average*	*b*/2 (Å)
Tuperssuatsiaite	M1: 2.063	T1: 1.615	M1: 58.2	M1: 2.174	T1: 111.5	2.254	8.921
	M2: 2.038	T2: 1.610	M2: 57.3	M2: 2.204	T2: 111.6		
	M3: 2.406		M3: 62.6	M3: 2.214			
Raite	M1: 2.074	T1: 1.623	M1: 57.0	M1: 2.259	T1: 112.4	2.241	8.800
	M2: 2.154	T2: 1.622	M2: 57.2	M2: 2.337	T2: 112.8		
	Na1: 2.400		Na1: 58.9	Na1: 2.482			
	Na2: 2.401		Na2: 60.06	Na2: 2.397			
	Ti: 2.291		Ti: 58.84	Ti: 2.371			

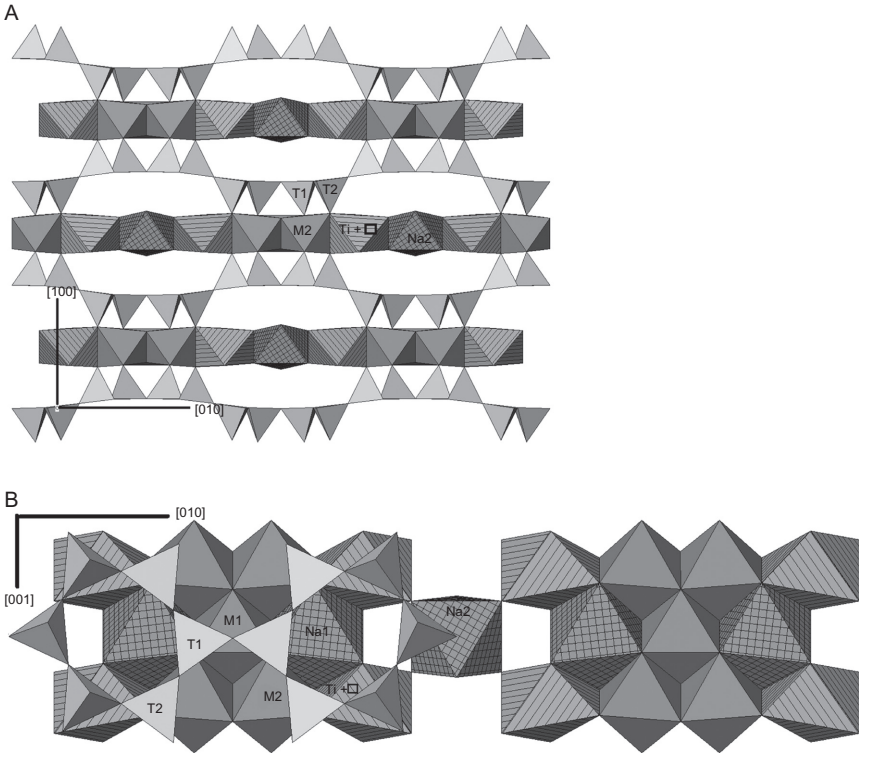

FIGURE 2 Raite (atomic data from Pluth et al., 1997) projected down the [001] direction in (A) and down [100] direction in (B). Light-filled triangles (yellow for online version) are Si tetrahedra, dark-fill octahedra (grey for online version) are Mn, cross-hatched, dark-fill octahedra (purple for online version) contain Na, and line-hatched, dark-fill (green for online version) octahedra contain Ti (0.45 per cell) and vacancies (0.55 per cell, signified in the label as a box). Part (B) better illustrates the discontinuous nature of the octahedral sheet because Na2 resides in the centre of the channel, and it is poorly linked to the octahedral ribbons via a site that contains mostly vacancies and some Ti. (For interpretation of the references to colour in this figure legend, the reader is referred to the Web version of this chapter.)

topology of the tetrahedral connectivity is sufficiently different that this mineral is not considered in detail here.

Kalifersite is believed to be composed of two polysomes: a palygorskite- and a sepiolite-like polysome. Ferraris et al. (1998) used a distance least-squares refinement procedure to show that the palygorskite–sepiolite polysome topology is consistent with the cell dimensions of kalifersite. This procedure optimized a set of atomic coordinates to match ideal bond distances, but the refinement process did not adjust atomic coordinates to fit a calculation with observed diffraction data. Comparison of the resultant atomic coordinates to powder X-ray data was poor, and Ferraris et al. (1998) attributed this result to poor crystallinity and preferred orientation of the sample in the X-ray beam.

However, an incorrect structure model could also explain a poor fit. Although a detailed X-ray study is probably not possible with the sample, a high-resolution transmission electron microscope study is likely to be useful.

In palygorskite and sepiolite, exchangeable cations, zeolitic H_2O, and vacant regions may reside in the channels in natural samples. Possible exchange reactions with organic molecules show that this exchange is dependent on the size of the organic cations because of steric constraints of the channels. One synthetic pigment (Maya Blue, used extensively by the Maya civilization because of its bright blue colour) involves the adsorption of the (organic) indigo molecule in palygorskite or sepiolite. Larger molecules also may be adsorbed by the structure, probably because of the existence of defects, which are discussed further below.

In palygorskite and sepiolite, the octahedral strips are terminated at the channel by four OH_2 per formula unit to form a part of the octahedral coordination polyhedron around Mg or Al (see details below). Raite is more complex and also has OH_2 (and H_2O) associated with octahedra and partially occupied octahedra in or next to the channel. In contrast, in tuperssuatsiaite, the octahedra at the strip edge contain Fe, Mn, or Na, and half the terminations involve OH groups and half involve OH_2 (Cámara et al., 2002).

Bailey (1980) related the two varieties of stacking (monoclinic, orthorhombic) of the palygorskite–sepiolite structures to the atomistic approach he used to derive the standard polytypes for the 2:1 layer phyllosilicates. Chisholm (1992) proposed atomic coordinates and space groups for these derived models. Within a polysome, the direction of shift of the upper tetrahedral strip may be either $+c/3$ or $-c/3$, depending on whether set I or set II octahedral cations occupy possible sites (the reader is referred to Bailey, 1980, p. 8, for the definition of set I and set II). The direction of shift or stagger of the upper tetrahedral strip in the polysome relative to the lower tetrahedral strip is based on closest packing within the polysome. Where the same set of octahedral cations is occupied from polysome to polysome (regardless if it is set I or set II), the direction of shift always remains the same and a monoclinic structure results (with an ideal $\beta = 105.2°$). Where alternation of shift directions occurs because set I alternates with set II in adjacent strips, an orthorhombic structure results ($\beta = 90°$). Because of the lack of precision of a Rietveld refinement over a single-crystal study, obtaining a reasonable structure with multiphase samples of closely related structures is especially difficult. For example, the three O_{apical}–T–O_{basal} angles describing the shape of a tetrahedron in the Giustetto and Chiari (2004) monoclinic palygorskite model vary between 83.1° and 119.8°. This is crystal chemically unreasonable because a large deviation from near 109.5° implies that the Si—O bond lacks significant covalent character. In contrast, however, the average of 106.9° is reasonably close to the ideal value of 109.5°. Similar problems exist for the orthorhombic palygorskite model.

2.4. Substitutions in Palygorskite and Sepiolite

Cation sites in the palygorskite–sepiolite group minerals are commonly defined from the centre of the octahedral strip, where there is often a special position such as a mirror plane, to the outer edge. For example, M1 is the central octahedral site on the special position, with M2 adjacent to M1, and M3 adjacent to M2 but further from the special position, etc. Tetrahedral cation sites are defined in a similar fashion.

In general, sepiolite is Mg rich and palygorskite has a ratio of Mg to R^{3+} cations from 3:1 to 1:3 and significant numbers of vacancies. Martin-Vivaldi and Cano-Ruiz (1955) and Drits and Aleksandrova (1966) surveyed the available (early) analytical data for palygorskite and found the data consistent with an octahedral sheet with a vacant site (one site vacant per five octahedra). Thus, sepiolite is primarily trioctahedral and palygorskite approaches dioctahedral. Because samples often contain impurities, obtaining accurate analyses are difficult (e.g. Smith and Norem, 1986). However, Galán and Carretero (1999) have shown that sepiolite can obtain near Mg end-member trioctahedral compositions of $Mg_8Si_{12}O_{30}(OH)_4(OH_2)_4(H_2O)_8$ and that palygorskite is intermediate between dioctahedral and trioctahedral with one of five octahedra vacant and the other octahedral sites occupied by Mg, Al, and Fe with R^{2+}/R^{3+} near 1.0. Although impurities may be an issue, Newman and Brown (1987) found that octahedral occupancy varied from $R^{3+}{}_{2.5}+R^{2+}{}_{1.5}$ for Al-rich specimens to $R^{3+}{}_{0.5}+R^{2+}{}_{4.25}$ for Mg-rich palygorskite. Tetrahedral occupancy is very Si rich with Al substitutions limited from $Al_{0.12}$ to $Al_{0.66}$ per eight T sites.

Serna et al. (1977), using infrared spectroscopy, and Heller-Kalai and Rozenson (1981), using infrared and Mössbauer spectroscopy, concluded that vacancies are ordered into M1 in palygorskite, and that Mg (and Fe) preferentially orders into M3. Chryssikos et al. (2009), also using infrared analysis, found that regions of the palygorskite structure were dioctahedral (with AlAlOH, $AlFe^{3+}OH$, $Fe^{3+}Fe^{3+}OH$ interactions) and trioctahedral (MgMgOH) regions, with these interactions implying that Al and Fe^{3+} order into M2. Based on average bond distances (see Table 2), Post and Heaney (2008) found vacancies ordered in M1, Al in M2, and Mg in M3, in accord with the spectroscopy studies and other Rietveld refinement studies (Artioli and Galli, 1994; Chiari et al., 2003; Giustetto and Chiari, 2004).

Although sepiolite is generally considered trioctahedral, sepiolite shows some octahedral vacancies (without ordering) where R^{3+} content is high with octahedral sums from 7.0 to 8.0 (Newman and Brown, 1987), with cations of mostly Mg and minor Mn, Fe^{3+}, Fe^{2+}, and Al. Tetrahedral content varies from ($Si_{11.96}Al_{0.05}$) to ($Si_{11.23}Fe^{3+}{}_{0.53}Al_{0.24}$), although R^{3+} content has been reported to be as high as 1.3 atoms per 12 sites (Bailey, 1980). Santaren et al. (1990) found a small substitution (1.3 wt.%) of F for OH ($\sim$25% of the OH groups) in a sepiolite from Spain.

2.5. H_2O, OH_2, and OH Positions in Palygorskite and Sepiolite

Hydrogen positions cannot be determined precisely from powder (Rietveld) X-ray data because the scattering efficiency of H is low for X-rays, even for higher quality material. Although this is not the case for neutron experiments, H positions may still be difficult to obtain accurately if the sample is poorly crystalline, as is generally the case for these minerals. Therefore, to determine the positions of the OH and OH_2 groups, only the oxygen atom location is used in most studies. For palygorskite, there is general agreement that the OH groups are part of the octahedral anion coordination of the M1 and M2 sites, which occur well within the octahedral strips (Figure 1). The OH_2 is part of the coordination unit around the M3 site along the edges of the octahedral strips, where the two hydrogen atoms are required for charge balance. For sepiolite, the OH groups are part of the inner octahedral strip coordinating to M1, M2, and M3, whereas the OH_2 groups are along the edges of the octahedral strip coordinating to M4, and this pattern is similar to that of palygorskite.

In contrast, locations for the zeolitic H_2O may vary depending on the Rietveld refinement being considered, and this may be a result of poor crystallinity, limitations of the refinement, and/or differences in chemical composition, including relative humidity. For (monoclinic) palygorskite, Post and Heaney (2008) found locations for two zeolitic H_2O molecules (or four H_2O per eight tetrahedral sites), which are consistent also with the molecular modelling results of Fois et al. (2003). One of these sites (H_2O2) is occupied only half the time (site locations are defined in Figure 1 and the zeolitic H_2O labels do not necessarily correspond to the labels in the original paper cited), based on both the refined occupancy factor of 0.5 and because adjacent H_2O2 sites are too close (1.03 Å) together to be occupied fully. This H_2O site is within hydrogen bonding distance (2.79, 2.93 Å) of the OH_2 site. The other H_2O molecule (H_2O1) resides on the mirror plane and shows significant positional disorder. In contrast, Giustetto and Chiari (2004) also located a third H_2O molecule in the channels of (monoclinic) palygorskite in a neutron Rietveld study of a deuterated sample containing both orthorhombic and monoclinic polytypes. They also found a more random network of hydrogen bonded H_2O molecules between the two polytypes. In summary, all refinements indicate a loosely held network of zeolitic H_2O molecules which account for the low temperatures of dehydration (e.g. <191 to $<247\,^{\circ}C$) and higher temperatures (~ 354–$510\,^{\circ}C$) that account for OH_2 and OH loss (thermal data from palygorskite, Florida, CMS Source clay PFl-1, Guggenheim and Koster van Groos, 2001). Dehydration (zeolitic H_2O loss) and dehydroxylation and OH_2 loss may partially overlap in temperature.

For sepiolite, Post et al. (2007) found four zeolitic H_2O molecules in a powder (Rietveld) synchrotron X-ray study. Two of the H_2O sites are approximately at full occupancy (H_2O1, H_2O2), one at near 0.5 occupancy

(H_2O3), and one (H_2O4) at about 0.3 occupancy, which produces about 15.6 zeolitic H_2O per 24 T sites (per unit cell). Hydrogen bond distances can vary considerably depending on the number of oxygen acceptor atoms linking to the hydrogen. However, the H_2O4 site, occupied at 0.3, is too close (1.64 Å) to adjacent H_2O4 sites to be occupied fully. This site, along with the H_2O2 site, is sufficiently close (2.41, 2.71 Å) to the OH_2 sites to be hydrogen bonded. The H_2O4 site is also sufficiently close (2.61 Å) to a framework oxygen atom to allow for hydrogen bonding.

2.6. Genetic and Synthesis Relations

The occurrences of palygorskite and sepiolite are discussed throughout this volume and are only summarized briefly here for the purposes of discussion below. Palygorskite and sepiolite are characterized as crystallizing from solution (e.g. Jones and Galán, 1988; Weaver, 1984) either in lacustrine (e.g. Chahi et al., 1997) or in perimarine (e.g. Singer, 1979; Velde, 1985; Weaver and Beck, 1977) environments. Additionally, crystallization may occur during diagenesis (e.g. Couture, 1977), or hydrothermally (e.g. Imai and Otsuka, 1984), although alteration from precursors such as smectite is also known (e.g. Singer, 1979; Yaalon and Wieder, 1976). Deep-ocean authigenic palygorskite and sepiolite near active ridge zones were described by Bowles et al. (1971). Jones and Galán (1988) summarized the occurrences of palygorskite and sepiolite in soils. They also tabulated a summary of the favourable environmental conditions of formation for palygorskite and sepiolite as compared to trioctahedral smectite (Table 4). At lower pH, palygorskite may form from amorphous silica and dioctahedral smectite, whereas at slightly higher pH, sepiolite, amorphous silica, and palygorskite can precipitate. Sepiolite is favoured over palygorskite at higher pH in silica-poor solutions (Birsoy, 2002). As expected, with high values of Al, Mg, and Si activity, palygorskite is favoured over sepiolite, but temporary variations in chemistry relating to changes in environmental conditions such as evaporation, rain, freshwater flow, etc. affect the formation of palygorskite and sepiolite (Garcia-Romero et al., 2007).

The rare members of the palygorskite–sepiolite group have more limited environmental conditions of formation. The type locality for kalifersite is the Khibina massif, Mt. Kukisvumchorr, Kola Peninsula, Russia, where the mineral is associated with hyperagpaitic (excess alkali) hydrothermally altered pegmatites (Ferraris et al., 1998). Ferraris et al. (1998) described the occurrence as "crystallization from residual peralkaline liquids during the hydrothermal stage of the pegmatic process". Raite occurs in pegmatite veins crossing an agpaitic nepheline syenite at Lovozero alkaline massif, Karnasurt Mountain, Kola Peninsula (Khomyakov, 1995; Pluth et al., 1997). These veins contain mineral assemblages that crystallized during early to late hydrothermal stages and epithermal stages, with raite found in cavities believed to

TABLE 4 Summary of Chemical Environments of Formation (after Jones and Galán, 1988) for Palygorskite (P), Sepiolite (S), and Trioctahedral smectite (TS).

Environmental conditions	Extent	Mineralogy
pH, alkalinity	pH < 8.5	+P, 0S, −TS
	PH = 8–9.5	0P, +S, 0TS
	PH > 9.5	−P, −S, +TS
Major element ratios	High (Mg + Si)/Al	0P, +S, −TS
	High (Mg + Fe)/Si	−P, −S, +TS
P(CO_2) of sediment water	High	−P, −S, +TS
	Low	+P, +S, −TS
Alkali salinity	High	−P, −S, +TS
	Intermediate	0P, +S, 0TS
	Moderate	+P, 0S, −TS

Symbols: +, favourable; 0, less favourable; −, absent.

originate from the last epithermal stage (Pluth et al., 1997). Tuperssuatsiaite was described from the Ilímaussaq alkaline complex in South Greenland (Karup-Møller and Peterson, 1984) and in other alkaline intrusive and extrusive rocks (Cámara et al., 2002). Falcondoite (Springer, 1976) was found in laterite deposits derived from a serpentinic harzburgite massif in the Dominican Republic, with veins primarily consisting of garnierite and sepiolite and limited falcondoite. In contrast, loughlinite occurs in veins in dolomitic oil shale replacing shortite, northupite, and searlesite (Fahey et al., 1960) in the Green River Formation, Wyoming, USA. This latter paragenesis suggests that loughlinite is an alteration product of the dolomitic marlstone from the saline zone of the Green River Formation. Yofortierite was described in agpaitic pegmatite veins (Perrault et al., 1975) in nepheline at Mont St. Hilaire. If intersilite (Yamnova et al., 1996) is included in the discussion for comparison, this mineral was described by Khomyakov (1995) from agpaitic–hydrothermal residual differentiates of an ultra-alkaline magma in the Lovozero alkaline massif, Kola Peninsula.

Experimental studies (La Iglesia, 1977; Siffert and Wey, 1962; Wollast et al., 1968) on palygorskite and sepiolite indicate that the conditions for synthesis involve a high activity of Si and Mg and high pH, with the availability of Al, favouring palygorskite over sepiolite (Hay and Wiggins, 1980; Singer and Norrish, 1974). Sepiolite (and kerolite) tends to form at lower Al activities, whereas palygorskite (and saponite) forms at higher Al activities

(Birsoy, 2002). Birsoy, using equilibrium activity diagrams, determined that direct precipitation of palygorskite and sepiolite is favoured at low values for log $[a\mathrm{Al}/(a\mathrm{H}^{+})^{3}]$, and he noted that palygorskite and sepiolite are more likely to be directly precipitated from solution in the presence of amorphous silica rather than quartz.

3. DISCUSSION OF STRUCTURE-RELATED TOPICS

3.1. Structure Parameters Described

To develop a context for the discussion of the palygorskite–sepiolite group minerals, structure parameters (Figure 3, Tables 2 and 3) are used here much like those used to describe phyllosilicate structures. The tetrahedral rotation angle, α, quantitatively describes the in-plane rotation of adjacent tetrahedra in opposite directions around the sixfold tetrahedral ring (Radolovich, 1961; Zvyagin, 1957). Tetrahedral rotation effectively reduces the lateral dimensions of an overly large Al-rich silicate tetrahedral sheet (in palygorskite–sepiolite minerals, these tetrahedra are Si rich only) to allow a fit for the apical oxygen atoms to coordinate the octahedral cations within a layer (or polysome). For palygorskite–sepiolite group members, there are two types of rings: those that are within the polysome, have tetrahedral apices pointing in one direction, and fit onto the continuous octahedral strip along the [001] direction ("polysome α"), and those that connect polysomes and involve the reversal of tetrahedral apices such that three tetrahedra point in one direction and three tetrahedra point in the opposite direction ("inter-polysome α"). The α value can be determined directly by measurement of relevant angles between tetrahedra.

Bailey (1980) described phyllosilicate structures as being composed of semi-elastic sheets. In addition to tetrahedral rotation, tetrahedral sheets further adjust their lateral dimensions either by thickening or by thinning. The value of 109.47 represents the ideal value for τ ($=\mathrm{O_{apical}}—\mathrm{T}—\mathrm{O_{basal}}$): $\tau > 109.47^{\circ}$ (thickening) reduces the apical oxygen atom to apical oxygen atom distance and $\tau < 109.47^{\circ}$ (thinning) increases the lateral dimension. Likewise, an octahedral coordination around a cation, M, has a comparable set of angles designated as ψ (ideal 54.73°) which is defined as the angle between the vertical (=octahedral thickness) and the octahedral body diagonal. Thus, cos ψ is calculated from (octahedral thickness)/[2(M—O, OH)], where M—O,OH is the average value of the bond distance for the octahedral site. The octahedral sheet is thinned, where ψ is greater than the ideal.

3.2. Structure Parameters and Tetrahedral–Octahedral Misfit

Modulated phyllosilicates, especially those with continuous octahedral sheets, are often described in terms of a misfit that originates because the lateral dimensions of the octahedral sheet are larger than the lateral dimensions of

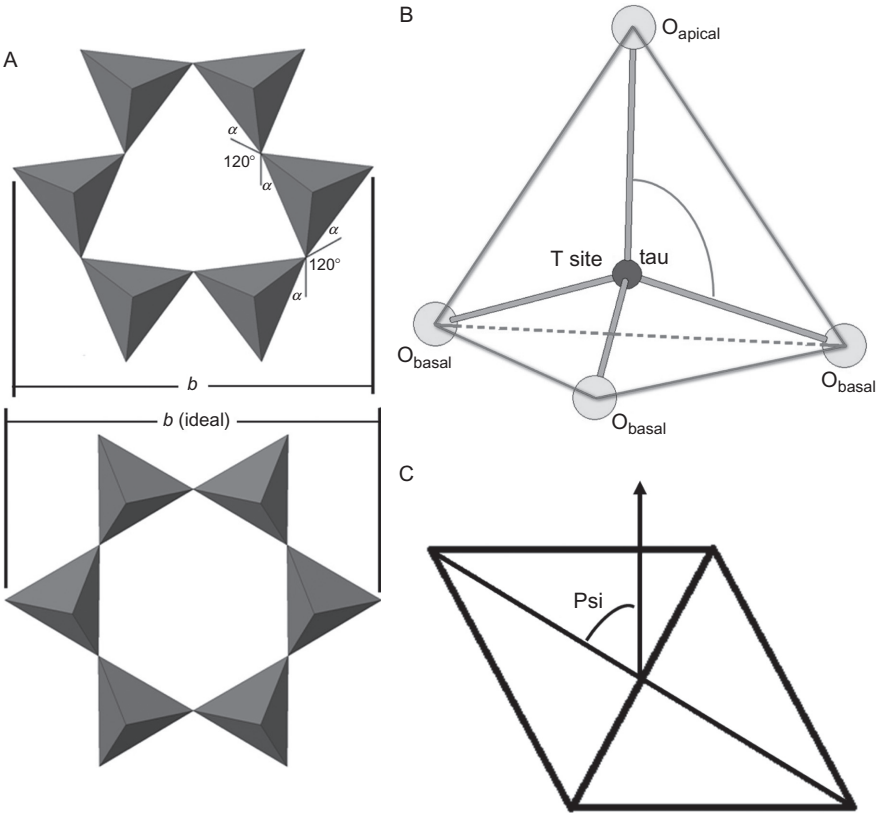

FIGURE 3 Structure parameters are used to quantify how a tetrahedral sheet or an octahedral sheet may adjust lateral dimensions to fit together. Panel (A) shows how an in-plane rotation of adjacent tetrahedra in opposite directions can reduce the lateral dimensions of an overly large tetrahedral sheet by deforming from hexagonal symmetry to a ditrigonal shape, in this case showing a reduction along *b*. The angle, α, can be measured directly from the atomic structure as shown. An α of zero implies that the tetrahedral sheet is at a maximum size. In (B), the angle, tau or τ, is defined. This angle is defined as the average of the three O_{apical}–T–O_{basal} angles. The ideal value in a perfect tetrahedron is 109.47°. Therefore, as this angle becomes larger than the ideal, the tetrahedron thickens (i.e. increases in height, as measured from the basal plane to O_{apical}). In (C), the angle, psi or ψ, is defined as between the octahedral body diagonal and the vertical (line with the arrow); the ideal value is 54.73°. Where this angle is greater than the ideal, the octahedron is thinner than ideal.

the adjacent (and linked) tetrahedral sheet (e.g. Bates, 1959; Guggenheim and Eggleton, 1987). As previously noted (Bailey, 1980; Guggenheim and Eggleton, 1988), misfit between these sheets does not seem to be a requirement for the tetrahedral inversions (modulations) in palygorskite and sepiolite. For example, if the channel occupancy is not considered, palygorskite (Post and Heaney, 2008) has a (weighted) average octahedral cation M—O bond

distance, including the large vacant site, of 2.016 Å and an average tetrahedral cation T—O bond distance of 1.623 Å. These values are consistent with those found in the micas (e.g. M: 2.019 Å, T: 1.632 Å, α: 7.3°, Guggenheim, 1981; M: 2.063, T: 1.625 Å, α: 1.4°, Toraya et al., 1976), which do not have modulations.

The parameter, *b*/2, represents the lateral size of the polysome (and the channel) or the width of the octahedra ribbon in palygorskite or sepiolite (where *b* is the cell dimension). This parameter (*b*/2) is not as strong an indicator of octahedral composition as *a*, for example, see Suárez et al. (2007). However, this ribbon width dictates the span of tetrahedra along the direction perpendicular to the ribbon direction. For palygorskite and similar structures, the ribbon width represents a span of four tetrahedra, and for sepiolite, the span is six tetrahedra. Thus, the magnitude of *b*/2 is a rough estimate of misfit (assuming all tetrahedra are Si rich). A *b*/2 value smaller than ideal implies that an out-of-plane tilt of tetrahedra occurs, in addition to any other structural compensation, such as tetrahedral rotation or sheet thinning or thickening. Palygorskite has a very uniform *b*/2 value, at 8.921–8.940 Å, and the structure appears to have a planar basal oxygen atom plane. Tuperssuatsiaite is similar, with a *b*/2 value of 8.921 Å. In contrast, sepiolite is slightly less compressed (at 9.005 Å when the value is normalized to four tetrahedra), and raite has the greatest compression (8.800 Å) and the greatest amount of out-of-plane tilt.

Although some misfit occurs in raite, it does not appear that a maximum strain (misfit) has been reached. The rotation angle in the polysome is 5.09° and the rotation angle between polysomes is 3.70°, and these values do not suggest fully extended tetrahedral rings to minimize overly large octahedra and a too small tetrahedral sheet. The ψ values for those octahedra linked to tetrahedral apices (M1, M2) are considerably larger than the ideal (at M1: 57.0°, M2: 57.2°), which indicates thinning, rather than the expected thickening, and τ values are larger than the ideal (at T1: 112.4°, T2: 112.8°), which indicates thickening, rather than the expected thinning, if misfit is being minimized.

In tuperssuatsiaite, the rotation angle in the polysome is 1.99° and the interpolysome rotation angle is 1.57°, and both these angles are close to the limits of fully extended rings, as noted by Cámara et al. (2002). However, the *b*/2 value is similar to that of palygorskite (no tetrahedral out-of-plane tilting), and the average octahedral size for octahedra that are linked to tetrahedral apices (M1, M2) is relatively small (M1, M2 average: 2.046 Å), considerably smaller than the relevant octahedra in raite (2.127 Å). Cámara et al. (2002) noted that M1 and M2 show substantial substitutions of R^{3+} cations (=Fe, Mn) and M2 may also contain Ti^{4+}, which explains the relatively small size of these sites. The τ angles (at T1: 111.5°, T2: 111.6°) are smaller than those found in raite and therefore more ideal (tetrahedra not as thick), although the tetrahedra are certainly not thin. The ψ values for octahedra linked to tetrahedral apices are larger than the ideal (at M1: 58.2°, M2: 57.3°, indicating thinning), and these values in tuperssuatsiaite are larger than that in raite.

In summary, palygorskite and sepiolite octahedral and tetrahedral sizes (i.e. effects of composition) are not much different than some micas which do not show modulations involving tetrahedral inversions. Even for the well-determined structures such as raite and tuperssuatsiaite, which are structurally similar to palygorskite, but compositionally different, structural parameters are not at their limits, which suggests that misfit does not play an important role in the formation of these minerals.

3.3. If Not Misfit, Why Do Polysomes Form?

In an early publication, Martin-Vivaldi and Cano-Ruiz (1955) suggested that the palygorskite–sepiolite structure may be favoured at certain ratios of octahedral cations to vacancies, that is, 4:1 in palygorskite and from (7 to 8): (1 to 0) in sepiolite, based on the idea that there may be structural discontinuities between dioctahedral and trioctahedral phyllosilicates. However, micas are now known to readily accommodate vacancy contents between dioctahedral and trioctahedral compositions, for example, see discussion in Guggenheim (1984, pp. 72–75). Thus, the argument that vacancy content is the reason for the palygorskite–sepiolite structure is without support. Without the view that inherent differences in the lateral extent of the octahedral and tetrahedral sheets are responsible for these structures, there is no prevailing view for why the palygorskite–sepiolite structure occurs instead of more traditional phyllosilicates, such as the smectite or mica group minerals.

Milton (1977) pointed out the similarity between the mineralogy of salt lakes (e.g. sepiolite and loughlinite in the Green River Formation) and alkalic igneous assemblages. Thus, the environment of formation (see above) of palygorskite–sepiolite group minerals ranges from low-temperature aqueous solutions (e.g. lacustrine and perimarine) to high-temperature hydrothermal (agpaitic). For lacustrine environments, palygorskite often forms in salt lakes from detrital material rich in aluminium, whereas sepiolite tends to precipitate further away from shore (Meunier, 2005). In a relatively Al-poor, high-temperature hydrothermal environment, the rare minerals (e.g. kalifersite, raite, tuperssuatsiaite) of the group are associated with agpaitic intrusions. These conditions indicate an alkali-rich $[(Na+K)/Al>1]$ aqueous environment at near-surface to hydrothermal ($<350\,^{\circ}C$) temperatures. In support of Milton (1977), Khomyakov (1995, p. 47) stated in reference to the agpaitic post-magmatic environments and soda lakes "...that the crystallization of minerals during the final stages of formation of the agpaitic nepheline syenites and the salt-bearing sediments took place under quite similar physicochemical conditions, in particular, with markedly increased alkalinity of the mineral-forming medium." Although Khomyakov (1995) stresses the similarities of the "physicochemical" conditions, a more precise statement may be that there is a continuum of environments, where the activity of (the components comprising) the polysomes, a_{polysome}, is similar.

Two important characteristics of the palygorskite–sepiolite group minerals are the continuous basal oxygen atom plane forming the tetrahedral linkages and the octahedral strips that forms polysomes. Of particular interest is that the octahedral strips are terminated by OH and OH_2 for anion completion of the octahedra at the polysome-channel interface. These terminations are consistent with an aqueous environment with a high a_{OH}. In contrast, trioctahedral smectite, either stevensite (Mg) or saponite (Al), forms also in aqueous environments at conditions similar to but not necessarily identical to palygorskite and sepiolite (Table 4, also see below). Clearly, the formation of smectite requires a high value of a_{OH} also. This suggests that unknown chemical parameters may affect the continuity of the octahedral sheet to produce either a palygorskite–sepiolite polysome or a traditional layer structure like smectite. This parameter may relate to a_{alkali}, a_{SiO_2}, and/or a_{OH}. In addition, a_{Mg} may be important because the activity of Mg affects and is affected by OH and Cl. To resolve these issues, more detailed experimental studies are required to define the conditions for polysome formation in the palygorskite–sepiolite group.

4. PART 2: MICROSTRUCTURE-RELATED TOPICS

Microtexture is a critical property of clay-sized materials because it strongly influences sorption behaviour, solubility, density, and many other fundamental properties involved in environmental interactions and industrial applications. Three broad types of defects occur in palygorskite, sepiolite, and yofortierite, and these are categorized as stacking errors, variation in the width of polysomes (and by extension transformation to montmorillonite), and omission of polysomes. These defects can be directly observed by transmission electron microscopy (TEM) techniques and to a lesser extent by atomic force microscopy (AFM) techniques.

TEM of palygorskite–sepiolite group minerals for microtexture study is challenging owing to the high H_2O content and the small crystallite size of most of these minerals, which make imaging and acquisition of selected area electron diffraction (SAED) data in the [100] direction difficult. Even with rapid (0.3–0.7 s) image capture by a charge-coupled device, beam damage of the sample is common. TEM data must be acquired with very low illumination.

4.1. Polysome-Width Disorder and the Transformation of Palygorskite to Smectite

Variation in the width of polysomes can commonly be observed from heavily streaked SAED patterns. Direct TEM imaging of variable width polysomes has been problematic owing to beam sensitivity of the sample. Krekeler and Guggenheim (2008) reported variable width in a sepiolite from Helsinki where quadruple-chain width polysomes were observed. Various widths of polysomes were also observed in yofortierite. Figure 4 shows images along

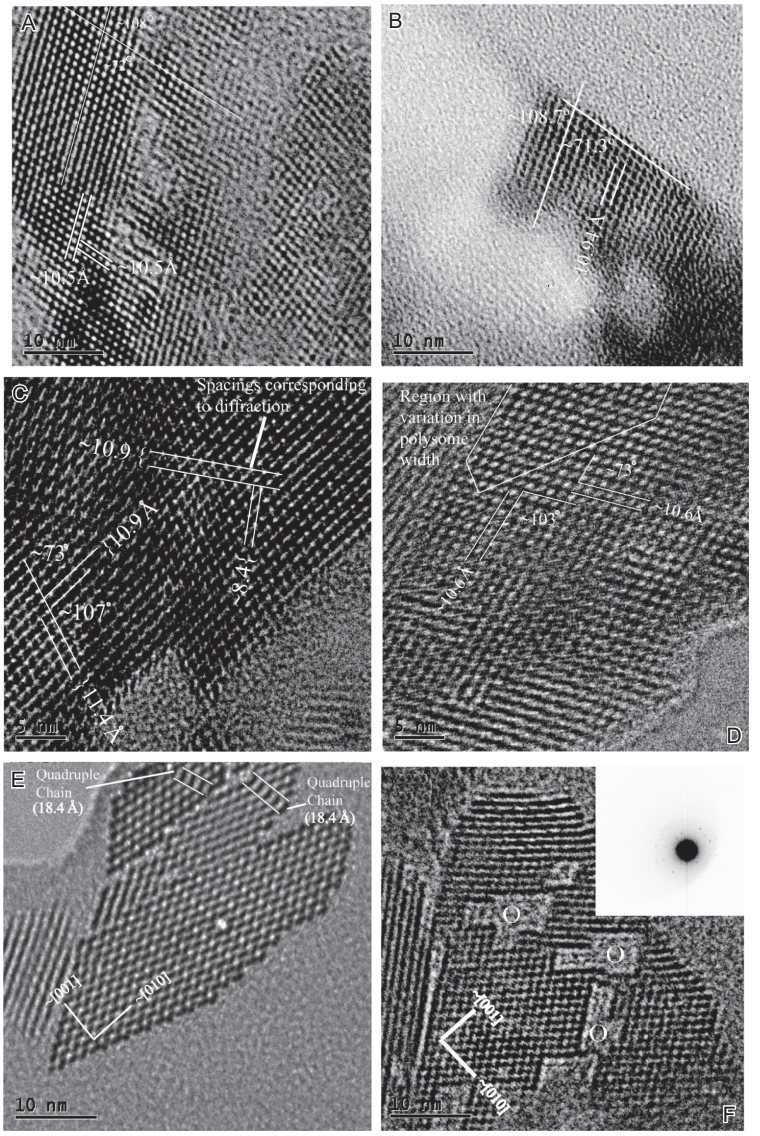

FIGURE 4 (A) TEM image of yofortierite along the [100] direction with significant beam damage in the right portion of the image. A parallelogram-like lattice is present where each side is approximately 10.5 Å, and the angles of the lattice are 72° and 108°. This spacing approximately corresponds to the 10.5-Å spacing of the (011) as determined by X-ray diffraction by Perrault et al. (1975). (B) TEM image of a single fibre in the [100] direction. The image shows parallelogram-like cleavage that is commonly observed in yofortierite. A parallelogram-like lattice is visible with a spacing of 10.94 Å with angles of 71.3° and 108.7°. (C) TEM image showing a parallelogram-like lattice is apparent with two similar but unequal spacings of 11.4 and 10.9 Å with angles of approximately 107° and 73°. (D) TEM image showing structural detail along the

the [100] direction of yofortierite with (A)–(C) showing images interpreted as being of dominantly regular polysome widths and image (D) showing a region interpreted as comprising irregular polysome widths. Although variations in polysome widths can be seen, it remains unclear whether these features are common in the palygorskite–sepiolite mineral group and correlate to geologic environments. Variation in polysome width may impact industrial mineral performance, and a better understanding of the nature of such variation is required for both mineralogical and applied reasons.

The transformation of palygorskite to smectite is related to polysome width disorder and has been studied or discussed by Golden and Dixon (1990), Merkl (1989), Golden et al. (1985), Güven and Carney (1979), and Randall (1956), and the transformation of smectite to palygorskite was identified in a TEM study by Chen et al. (2004). Transformations of palygorskite to and from smectite are further evidence of the importance of chemical parameters in affecting the continuity of the octahedral sheet rather than purely structural parameters (e.g. misfit, see above). Golden and Dixon (1990) showed a close textural association of smectite and palygorskite from a series of experiments using TEM data. Their work indicated that palygorskite readily converts to smectite above 100 °C, although the reaction was sluggish at room temperature (22 °C). They showed that at conditions near a pH of 12, the palygorskite to smectite transformation occurs over a period of several months. Merkl (1989) investigated textural relationships of palygorskite, smectite, and kaolinite, in material from the Meigs Member and the Dogtown Clay Member of the Hawthorne Formation in southern Georgia (USA) using scanning electron microscopy (SEM) techniques. This work suggested that a transformation between palygorskite and smectite may exist in these sediments; however, the SEM data were insufficient in spatial resolution to definitively identify a transformation. Golden et al. (1985) conducted experiments with solutions at 150 °C which produced smectite from palygorskite. TEM data from grain mounts showed clear alteration textures of palygorskite fibres

[100] direction. The lower right portion of the image is a grain boundary between the yofortierite fibre and amorphous carbon film. The extreme upper left of the image is a beam-damaged yofortierite particle not in the same orientation as the central portion of the image. Structural information in the image is most pronounced in the upper central portion. A parallelogram-like lattice pattern is present with a spacing of approximately 10.6 Å and angles of 73° and 103°. Widths of white regions in the image vary, which may be related to widths of either channels or polysomes. (E) TEM image along [100] of sepiolite from Helsinki showing a strip of 18.4 Å wide features consistent with quadruple-chain width polysomes. (F) Image approximately along the [100] direction of a yofortierite fibre. This image has a rhombus-like lattice fringe contrast with a spacing of approximately 10.8 Å, a value consistent with the (011) spacing from X-ray diffraction (Perrault et al., 1975). OCD regions (labelled O) are rhombus- and parallelogram-like in shape and vary in cross-sectional area from approximately 16 to 75 nm^2. The limited selected area electron diffraction (SAED) data suggest that this is a single crystal.

and an intimate association of smectite with reacted palygorskite fibres, and these observations suggest a dissolution–reprecipitation process. Güven and Carney (1979) found in hydrothermal experiments that NaCl increased the rate of formation of stevensite at temperatures below 260 °C, and from 260 to 316 °C sepiolite transformed to stevensite independent of ionic strength of the solution. This body of work clearly defines a process, although details on the specific nature of the structural transformation were not provided.

The transformation of palygorskite to smectite was investigated in detail using AFM and TEM techniques on natural samples by Krekeler et al. (2005) using materials from a paleohydrologic horizon from the Meigs Member of the Hawthorne Formation, southern Georgia, USA. AFM investigation indicated that palygorskite fibres in this horizon were commonly altered. Many AFM images of the altered fibres showed an oriented overgrowth of platy morphology, which was interpreted as smectite. This latter mineral forms along the length of the palygorskite crystals with an interface parallel to {010} of the palygorskite. The resulting grains have an elongate "wing-like" morphology. TEM imaging shows smectite lattice-fringe lines that are intergrown with 2:1 layer ribbon polysomes of fibres (Figure 5). The polysomes involved in these textures commonly are of variable widths that are consistent with double-tetrahedral chains (10.4 Å), triple-tetrahedral chains (14.8 Å), quadruple-tetrahedral chains (21.7 Å), and quintuple-tetrahedral chains (24.5 Å). These lattice-fringe lines indicate an epitaxial overgrowth of smectite on palygorskite fibres. They also illustrate the structural relationship between platy overgrowths on fibres observed in AFM data. This epitaxial relationship may be described as {010} [001] palygorskite ‖ {010} [001] smectite.

The transformation of palygorskite to montmorillonite and the resulting intergrowths are expected to cause variations in bulk physical properties of palygorskite-rich clays, which may have important crystal chemical (and industrial) and geologic implications. For example, the variable widths of the polysomes would be expected to accommodate organic molecules of corresponding size. Hence, the sorptive properties of palygorskite may be affected by large molecules that are accommodated in (larger) defect interstices (see below also). Therefore, the sorptive properties may not be limited to molecules that fit only in the ideal palygorskite structure where the polysomes are two pyroxene-like chains wide. If future research shows that defects affect sorption properties significantly, then industrial applications such as pesticide carriers, filtering, cleaning products, etc. may be enhanced. The transformation may also account for the very low abundance of palygorskite found in Mesozoic and older sediments. An implication of the transformation is that palygorskite deposits may have existed in abundance in Mesozoic and perhaps even older sedimentary systems.

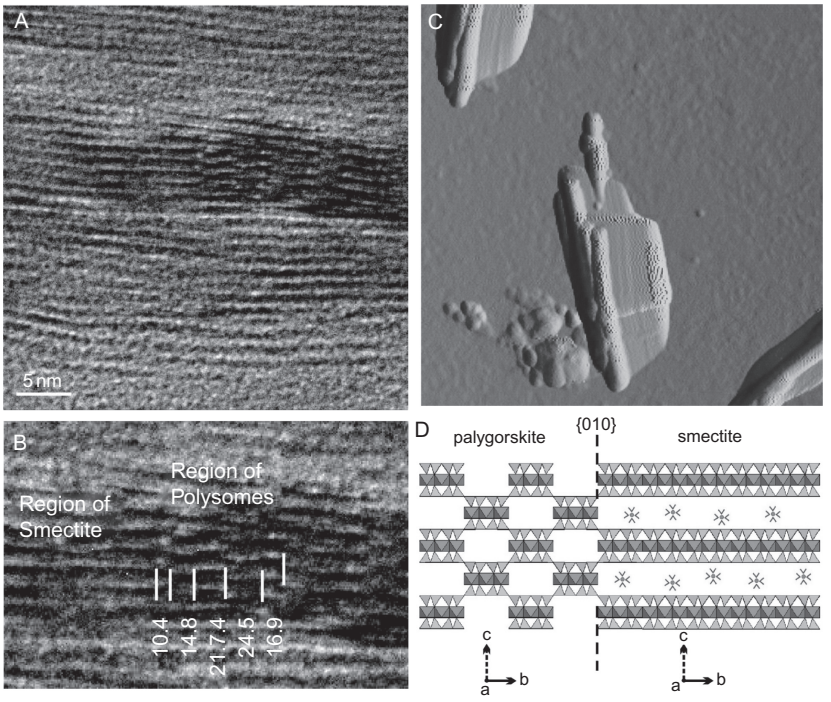

FIGURE 5 TEM images of palygorskite–smectite intergrowth. (A) Unlabelled image with parallel to sub-parallel lattice fringes (montmorillonite) surrounding rectangular blocks arranged in a regular or nearly regular manner (ribbons) in the centre right portion of the image. (B) Enlargement of the transition zone between a region of smectite and a region of polysomes with variable ribbons widths labelled in Ångströms. The image is approximately along the [100]. (C) AFM image (height data) of particles dispersed on a mica substrate. Acicular crystals are interpreted as palygorskite with "wing-like" overgrowths of montmorillonite. (D) Structural schematic of the epitaxial relationship between palygorskite and smectite overgrowths; {010} [001] palygorskite ‖ {010} [001] smectite. Figure from Krekeler et al. (2005) and reprinted with permission of The Clay Minerals Society, publisher of *Clays and Clay Minerals*.

4.2. Open Channel Defects

In addition, open channel defects (OCDs) were commonly observed in sepiolite from Helsinki and yofortierite from Mont St. Hillaire. These defects consist of omission of single or multiple polysomes in a fibre (hereafter referred to as OCDs), both as isolated occurrences in single fibres (Figure 6) and as dense groups. The cross-sectional area of OCDs varies greatly from approximately 3.9 nm^2 for a single omission to as much as 75 nm^2 for multiple polysome omission in yofortierite.

The specific cause of OCD formation is currently unclear; however, structures may result from rapid crystallization. OCDs may possibly arise by changes in direction of crystal growth where (011) faces coalesce during

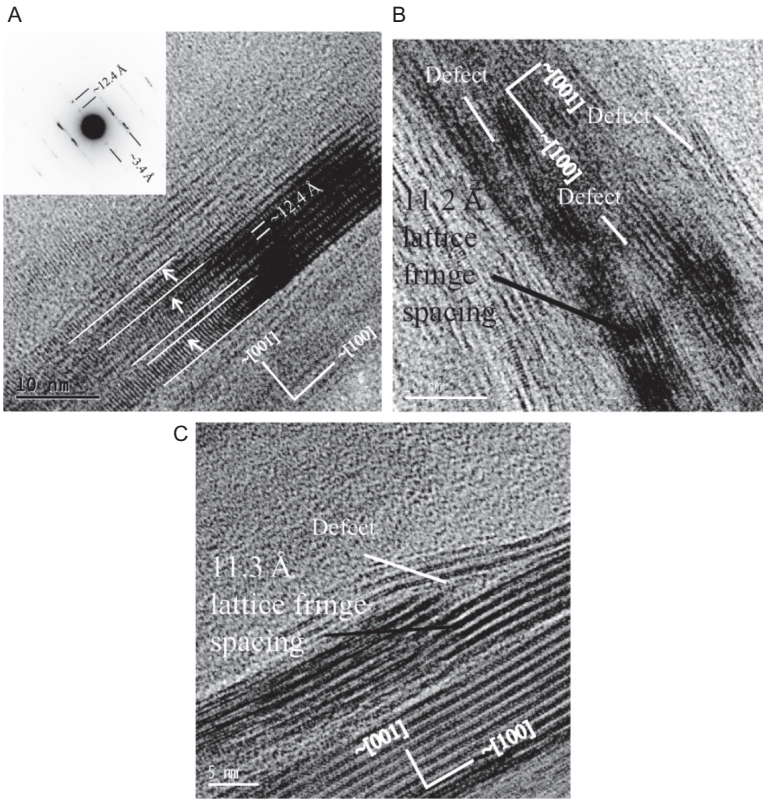

FIGURE 6 (A) TEM image of yofortierite along the [010] direction showing examples of stacking disorder of polysomes. Inset SAED pattern shows streaking along the *c* axis. (B) TEM image of a palygorskite fibre from the Hawthorne Formation exhibiting a planar-angular defect near the centre of the crystal. The image is taken approximately along the [010] direction. (C) TEM image of palygorskite fibre from the Hawthorne Formation along the [010] direction showing a planar-angular defect at a palygorskite fibre edge. Figure from Krekeler and Guggenheim (2008).

crystallization to produce large channels several tens of nanometres wide. Krekeler and Guggenheim (2008) interpreted this as a possible mechanism for the formation of OCDs occurring in the fibrous sepiolite from Helsinki. Progressive stages of OCD formation were observed.

The presence or absence of OCDs is expected to have a strong control on the variations in H_2O content in palygorskite and sepiolite. For example, differential thermal analysis (DTA) techniques show variations commonly of 2–7 wt.% H_2O from palygorskite and sepiolite (e.g. Jones and Galán, 1988). The H_2O molecules residing in OCD structures may account for this variation, and palygorskite and sepiolite with anomalously high H_2O content may be rich in OCD structures.

Conflicting reports exist regarding the nature of sorption and interaction of large organic molecules, such as cationic dyes and aromatic hydrocarbons, with the channels of palygorskite and sepiolite (e.g. Jones and Galán 1988; Ruiz-Hitzky, 2001). The primary issue is whether large organic molecules can fully exchange and replace cations and H_2O in the channels. The organic molecule exchanged in palygorskite and sepiolite requires a seemingly ordered transfer in the linear geometry of the confined channels along the [100] direction. An efficient mechanism for transport of large organic molecules and expulsion of at least some zeolitic H_2O molecules through a fibre length (a minimum of several hundreds to thousands of Ångströms, Jones and Galán, 1988) of channels seems problematic. However, large organic molecules have been reported to exchange in the channels of palygorskite and sepiolite (e.g. Jones and Galán, 1988; Ruiz-Hitzky, 2001; Serna and Fernandez-Alvarez, 1974). The determination of this exchange is primarily based on infrared spectroscopy, DTA, and other related techniques (e.g. Ruiz-Hitzky, 2001).

The presence of OCD structures in palygorskite and sepiolite may partly explain why some samples absorb large molecules and others do not. OCD structures or channels resulting from the occurrence of wide polysomes would enable geometric configurations consistent with exchange. Further, OCD structures and wide channels may enable zeolitic H_2O molecules to be more mobile during exchange with organic molecules, potentially affecting the kinetics of exchange.

4.3. Stacking Errors and Planar Defects

Defects relating to orientation of 2:1 ribbons are very common in palygorskite and sepiolite and fall into two broad groups: stacking errors and planar defects. Stacking errors are 180° rotations of 2:1 ribbons with respect to each other along the *c* axis, and these errors may be observed along the [010] of fibres often as cross-fringes in the TEM. Figure 6A shows stacking errors indicated by arrows. These cross-fringes are interpreted to represent the orientation of groups of 2:1 layer ribbon polysomes. Four regions in the fibre are shown, left to right with groups of 3, 4, 1, and 3 coherently oriented polysomes. The inset SAED pattern shows streaking in the stacking direction parallel to the c^* axis.

Planar defects such as these are common in palygorskite and sepiolite fibres and are characterized by 2–5° offsets normal to [001]. Common lengths are 75–125 nm along the [100] direction, and displacements generally are one to four lattice fringes. These defects are most common in fibres that are 50–100 nm in width. Palygorskite fibres from the Miocene Hawthorne Formation have larger angular deviations being approximately 8–16° normal to [001]. Planar defects of this type are common and occur in approximately 10–15% of these palygorskite fibres. Figure 6C is a TEM image of an edge of a palygorskite fibre approximately along [010] with lattice-fringe spacings

of approximately 11.3 and 3.2 Å. Near the centre of the image, lattice fringes indicate a planar defect, and these fringes are oriented approximately 16° from the lattice fringes of the fibre interior. Such defects are common in palygorskite fibres from the Hawthorne Formation, occurring in approximately 3–5% of fibres in the Pittman quarry samples.

Establishing a more detailed understanding of the nature of defects is critical for refining and developing industrial applications. More detailed TEM investigations of the palygorskite–sepiolite group are needed for comparative study.

ACKNOWLEDGEMENTS

We thank P. Heaney, Pennsylvania State University, A. F. Koster van Groos, University of Illinois at Chicago, and an anonymous reviewer for comments on the chapter.

REFERENCES

Artioli, G., Galli, E., 1994. The crystal structures of orthorhombic and monoclinic palygorskite. Mater. Sci. Forum 166–169, 647–652.

Artioli, G., Galli, E., Burattini, E., Cappuccio, G., Simeoni, S., 1994. Palygorskite from Bolca, Italy: a characterization by high-resolution synchrotron radiation powder diffraction and computer modeling. Neues Jahrb. Mineral. Monatsh. 5, 217–229.

Bailey, S.W., 1980. Structures of layer silicates. In: Brindley, G.W., Brown, G. (Eds.), Crystal Structures of Clay Minerals and Their X-ray Identification. Mineralogical Society, London, England, pp. 1–124.

Bates, T.F., 1959. Morphology and crystal chemistry of 1:1 layer lattice silicates. Am. Mineral. 44, 78–114.

Birsoy, R., 2002. Formation of sepiolite-palygorskite and related minerals from solution. Clays Clay Miner. 50, 736–745.

Bowles, A., Angino, E.A., Hosterman, J.W., Galle, O.K., 1971. Precipitation of deep-sea palygorskite and sepiolite. Earth Planet. Sci. Lett. 11, 324–332.

Bradley, W.F., 1940. The structural scheme of attapulgite. Am. Mineral. 25, 405–410.

Cámara, F., Garvie, L.A.J., Devouard, B., Groy, T.L., Buseck, P.R., 2002. The structure of Mn-rich tuperssuatsiaite: a palygorskite-related mineral. Am. Mineral. 87, 1458–1463.

Chahi, A., Fritz, B., Duplay, J., Weber, F., Lucas, J., 1997. Textural transition and genetic relationship between precursor stevensite and sepiolite in lacustrine sediments (Jbel Rhssoul, Morocco). Clays Clay Miner. 45, 378–389.

Chen, T., Xu, H., Lu, A., Xu, X., Peng, S., Yue, S., 2004. Direct evidence of transformation from smectite to palygorskite: TEM investigation. Sci. China D Earth Sci. 47, 985–994.

Chiari, G., Giustetto, R., Ricchiardi, G., 2003. Crystal structure refinements of palygorskite and Maya Blue from molecular modeling and powder synchrotron diffraction. Eur. J. Mineral. 15, 21–33.

Chrisholm, J.E., 1992. Powder diffraction patterns and structural models for palygorskite. Can. Mineral. 30, 61–73.

Christ, C.L., Hathaway, J.C., Hostetler, P.B., Shepard, A.O., 1969. Palygorskite: new X-ray data. Am. Mineral. 54, 198–205.

Chryssikos, G.D., Gionis, V., Kacandes, G.H., Stathopoulou, E.T., Suárez, M., García-Romero, E., et al., 2009. Octahedral cation distribution in palygorskite. Am. Mineral. 94, 200–203.

Couture, R.A., 1977. Composition and origin of palygorskite-rich and montmorillonite-rich zeolite-containing sediments from the Pacific Ocean. Chem. Geol. 19, 113–130.

de Lapparent, J., 1935. Sur un constituent essential des terres a foulon. C. R. Acad. Sci. Paris 201, 481–482.

Dowty, E., 2005. ATOMS for Windows. Shape Software, Kingsport, TN, USA.

Drits, V.A., Aleksandrova, V.A., 1966. On the crystallographic nature of palygorskite. Zap. Vses. Miner. Obshch. 95, 551–560.

Drits, V.A., Sokolova, G.V., 1971. Structure of palygorskite. Sov. Phys., Crystallogr. 16, 183–185.

Fahey, J.J., Ross, M., Axelrod, J.M., 1960. Loughlinite, a new hydrous sodium magnesium silicate. Am. Mineral. 45, 270–281.

Ferraris, G., Khomyakov, A.P., Belluso, E., Soboleva, S.V., 1998. Kalifersite, a new alkaline silicate from Kola Peninsula (Russia) based on the palygorskite-sepiolite polysomatic series. Eur. J. Mineral. 10, 865–874.

Fois, E., Gamba, A., Tilocca, A., 2003. On the unusual stability of Maya Blue paint: molecular dynamics simulations. Microporous Mesoporous Mater. 57, 263–272.

Galán, E., Carretero, M.I., 1999. A new approach to compositional limits for sepiolite and palygorskite. Clays Clay Miner. 47, 399–409.

Garcia-Romero, E., Suárez, M., Santarén, J., Alvarez, A., 2007. Crystal chemical characterization of the palygorkite andsepiuolite from the Allou Kagne deposit, Senegal. Clays Clay Miner. 55, 606–617.

Giustetto, R., Chiari, G., 2004. Crystal structure refinement of palygorskite from neutron powder diffraction. Eur. J. Mineral. 16, 521–532.

Golden, D.C., Dixon, J.B., 1990. Low temperature alteration of palygorskite to smectite. Clays Clay Miner. 38, 401–408.

Golden, D.C., Dixon, J.B., Shadfar, H., Kippenberger, L.A., 1985. Palygorskite and sepiolite alteration to smectite under alkaline conditions. Clays Clay Miner. 33, 44–50.

Guggenheim, S., 1981. Cation ordering in lepidolite. Am. Mineral. 66, 1221–1232.

Guggenheim, S., 1984. The brittle micas. In: Bailey, S.W. (Ed.), Micas. Reviews in Mineralogy, vol. 13. Mineralogical Society of America, Washington, DC, pp. 61–104.

Guggenheim, S., 2010. Structures of the palygorskite-sepiolite group minerals: comments on the formation of the polysomes. In: Book of abstracts of the General Meeting. 2010 SEA-CSSJ-CMS Trilateral Meeting on Clays, p. 38.

Guggenheim, S., Eggleton, R.A., 1987. Modulated 2:1 layer silicates: review, systematics, and predictions. Am. Mineral. 72, 724–738.

Guggenheim, S., Eggleton, R.A., 1988. Crystal chemistry, classification, and identification of modulated layer silicates. In: Bailey, S.W. (Ed.), Hydrous Phyllosilicates (Exclusive of the Micas). Reviews in Mineralogy, vol. 20. Mineralogical Society of America, Washington, DC, pp. 675–725.

Guggenheim, S., Koster van Groos, A.F., 2001. Baseline studies of the clay minerals society source clays: thermal analysis. Clays Clay Miner. 49, 433–443.

Guggenheim, S., Adams, J.M., Bain, D.C., Bergaya, F., Brigatti, M.F., Drits, V.A., et al., 2006. Summary of recommendations of nomenclature committees relevant to clay mineralogy: report of the Association Internationale pour l'Etude des Argiles (AIPEA) Nomenclature-Committee for 2006. Clays Clay Miner. 54, 761–772 and Clay Minerals, 41, 863–878.

Güven, N., Carney, L.L., 1979. The transformation of sepiolite to stevensite and the effect of added chloride and hydroxide. Clays Clay Miner. 27, 253–260.

Hay, R.L., Wiggins, B., 1980. Pellets, ooids, sepiolite and silica in three calcretes of the southwestern United States. Sedimentology 27, 559–576.

Heller-Kalai, L., Rozenson, I., 1981. Mössbauer studies of palygorskite and some aspects of palygorskite mineralogy. Clays Clay Miner. 29, 226–232.

Imai, N., Otsuka, R., 1984. Sepiolite and palygorskite in Japan. In: Singer, A., Galán, E. (Eds.), Palygorskite-Sepiolite. Occurrences, Genesis, and Uses. Developments in Sedimentology, vol. 37. Elsevier, Amsterdam, pp. 211–232.

Jones, B.F., Galán, E., 1988. Sepiolite and palygorskite. In: Bailey, S.W. (Ed.), Hydrous Phyllosilicates (Exclusive of the Micas). Reviews in Mineralogy, vol. 19. Mineralogical Society of America, Washington, DC, pp. 631–674.

Karup-Møller, S., Peterson, O.V., 1984. Tuperssuatsiaite, a new mineral species from the Ilímaussaq intrusion in South Greenland. Neues Jahrb. Mineral. Monatsh. 501–512.

Khomyakov, A.P., 1995. Mineralogy of Hyperagpaitic Alkaline Rocks. Clarendon, Oxford.

Krekeler, M.P.S., Guggenheim, S., 2008. Defects in microstructure in palygorskite-sepiolite minerals: a transmission electron microscopy (TEM) study. Appl. Clay Sci. 39, 98–105.

Krekeler, M.P.S., Hammerly, E., Rakovan, J., Guggenheim, S., 2005. Microscopy studies of the palygorskite to smectite transformation. Clays Clay Miner. 53, 94–101.

La Iglesia, A., 1977. Precipitación por disolución homogénea de silicatos de aluminio y magnesio a temperatura ambiente. Sintesis de la paligorskita. Estud. Geol. 33, 535–544.

Martin, R.T., Bailey, S.W., Eberl, D.D., Fanning, D.S., Guggenheim, S., Kodama, H., et al., 1991. Revised classification of clay materials: report of the Clay Minerals Society Nomenclature Committee for 1986–1988. Clays Clay Miner. 39, 333–334.

Martin-Vivaldi, J.L., Cano-Ruiz, J., 1955. Contribution to the study of sepiolite: II. Some considerations regarding the mineralogical formula. Clays Clay Miner. 4, 173–176.

Merkl, R.S., 1989. A sedimentological, mineralogical, and geochemical study of the fuller's earth deposits of the Miocene Hawthorne group of south Georgia-north Florida. Ph.D. Dissertation, Indiana University, Bloomington, Indiana 182p.

Meunier, A., 2005. Clays. Springer, Berlin.

Milton, C., 1977. Mineralogy of the Green River Formation. Mineral. Rec. 8, 368–379.

Newman, A.C.D., Brown, G., 1987. The chemical constitution of clays. In: Newman, A.C.D. (Ed.), Chemistry of Clays and Clay Minerals. Monograph, vol. 6. Mineralogical Society, London, England, pp. 1–128.

Perrault, G., Harvey, Y., Pertsowsky, R., 1975. La yofortierite, un nouveau silicate hydrate de manganèse de St-Hilaire, P.Q.. Can. Mineral. 13, 68–74.

Pluth, J.J., Smith, J.V., Pushcharovsky, D.Y., Semenov, E.I., Bram, A., Riekel, C., et al., 1997. Third-generation synchrotron x-ray diffraction of a 6-μm crystal of raite, $\sim Na_3Mn_3Ti_{0.25}Si_8O_{20}(OH)_{2.10}H_2O$, opens up new chemistry and physics of low-temperature minerals. Proc. Natl. Acad. Sci. USA 94, 12263–12267.

Post, J.E., Bish, D.L., 1989. Rietveld refinement of crystal structures using powder X-ray diffraction data. In: Bish, D.L., Post, J.E. (Eds.), Modern Powder Diffraction. Reviews in Mineralogy, vol. 20. Mineralogical Society of America, Washington, DC, pp. 277–308.

Post, J.E., Heaney, P.J., 2008. Synchrotron powder X-ray diffraction study of the structure and dehydration behavior of palygorskite. Am. Mineral. 93, 667–675.

Post, J.E., Bish, D.L., Heaney, P.J., 2007. Synchrotron powder X-ray diffraction study of the structure and dehydration behavior of sepiolite. Am. Mineral. 92, 91–97.

Radolovich, E.W., 1961. Surface symmetry and cell dimensions of layer lattice silicates. Nat. Lond. 191, 67–68.

Randall, B.A.O., 1956. Stevensite from the Whin Sill in the region of the North Tyne. Mineral. Mag. 32, 218–229.

Robertson, R.H.S., 1962. The acceptability of mineral group names. Clay Miner. Bull. 5, 41–43.

Ruiz-Hitzky, E., 2001. Molecular access to intracrystalline tunnels of sepiolite. J. Mater. Chem. 11, 86–91.

Santaren, J., Sanz, J., Ruiz-Hitsky, E., 1990. Structural fluorine in sepiolite. Clays Clay Miner. 38, 63–68.

Serna, C., Fernandez-Alvarez, T., 1974. Adsorcion de hidrocarburos en sepiolite II: Propiedades ed superficie. Anal. Quim. 71, 371–376.

Serna, C., VanScoyoc, G.E., Ahlrichs, J.L., 1977. Hydroxyl groups and water in palygorskite. Am. Mineral. 62, 784–792.

Siffert, B., Wey, R., 1962. Synthèsis d'une sépiolite à température ordinaire. C. R. Acad. Sci. Paris 245, 1460–1463.

Singer, A., 1979. Palygorskite in sediments: detrital, diagenetic, or neoformed. A critical review. Geol. Rundsch. 68, 996–1008.

Singer, A., Norrish, K., 1974. Pedogenetic palygorskite. Occurrences in Australia. Am. Mineral. 59, 508–517.

Smith, D.G.W., Norem, D., 1986. The electron microprobe analysis of palygorskite. Can. Mineral. 24, 499–511.

Springer, G., 1976. Falcondoite, nickel analogue of sepiolite. Can. Mineral. 14, 407–409.

Ssaftschenkow, T.V., 1862. Palygorskit. Verhandlungen der Russisch Kaiserlichen Gesellschaft für Mineralogie, Sankt Petersburg 102–104.

Suárez, M., García-Romero, E., Sánchez del Río, M., Martinetto, P., Dooryhée, E., 2007. The effect of the octahedral cations on the dimensions of the palygorskite cell. Clay Miner. 42, 287–297.

Toraya, H., Iwai, S., Marumo, F., Daimon, M., Kondo, R., 1976. The crystal structure of tetrasilicic potassium fluor mica $KMg_{2.5}Si_4O_{10}F_2$. Z. Kristallogr. 148, 65–81.

Velde, B., 1985. Clay minerals: a physico-chemical explanation of their occurrence. Developments in Sedimentology, vol. 40. Elsevier, New York, p. 427.

Weaver, C.E., 1984. Origin and geologic implications of the palygorskite of S.E. United States. In: Singer, A., Galán, E. (Eds.), Palygorskite-Sepiolite. Occurrences, Genesis, and Uses. Developments in Sedimentology, vol. 37. Elsevier, Amsterdam, pp. 39–58.

Weaver, C.E., Beck, K.C., 1977. Miocene of the S.E. United States: a model for chemical sedimentation in a perimarine environment. Sediment. Geol. 17, 1–234.

Wollast, R., Mackenzie, F.T., Bricker, O., 1968. Experimental precipitation and genesis of sepiolite at earth-surface conditions. Am. Mineral. 53, 1645–1662.

Yaalon, D.M., Wieder, M., 1976. Pedogenetic palygorskite in some arid brown (caliothid) soils of Israel. Clay Miner. 11, 73–79.

Yamnova, N.A., Egorov-Tismenko, Yu.K., Khomyakov, A.P., 1996. Crystal structure of a new natural (Na,Mn,Ti)-phyllosilicate. Crystallogr. Rep. 41, 239–244 as translated from the Russian in: Kristallografiya (1996) 41, 257–262.

Zoltai, T., 1981. Amphibole asbestos mineralogy. In: Veblen, D.R. (Ed.), Amphiboles and Other Hydrous Pyriboles. Reviews in Mineralogy, vol. 9A. Mineralogical Society of America, Washington, DC, pp. 237–278.

Zvyagin, B.B., 1957. Determination of the structure of celadonite by electron diffraction. Sov. Phys. Crystallogr. 2, 388–394.